ACS Chemical Neuroscience

pubs.acs.org/chemneuro Research Article

Atomic Insights into Amyloid-Induced Membrane Damage

Yanxing Yang, Hannah Distaffen, Sharareh Jalali, Andrew J. Nieuwkoop, Bradley L. Nilsson, and Cristiano L. Dias*

Cite This: ACS Chem. Neurosci. 2022, 13, 2766−2777 Read Online

ACCESS | Metrics & More | Article Recommendations | Supporting Information

ABSTRACT: Amphipathic peptides can cause biological membranes to leak either by dissolving their lipid content via a detergent-like mechanism or by forming pores on the membrane surface. These modes of membrane damage have been related to the toxicity of amyloid peptides and to the activity of antimicrobial peptides. Here, we perform the first all-atom simulations in which membrane-bound amphipathic peptides self-assemble into β-sheets that subsequently either form stable pores inside the bilayer or drag lipids out of the membrane surface. An analysis of these simulations shows that the acyl tail of lipids interact strongly with non-polar side chains of peptides deposited on the membrane. These strong interactions enable lipids to be dragged out of the bilayer by oligomeric structures accounting for detergent-like damage. They also disturb the orientation of lipid tails in the vicinity of peptides. These distortions are minimized around pore structures. We also show that membrane-bound β-sheets become twisted with one of their extremities partially penetrating the lipid bilayer. This allows peptides on opposite leaflets to interact and form a long transmembrane β-sheet, which initiates poration. In simulations, where peptides are deposited on a single leaflet, the twist in β-sheets allows them to penetrate the membrane and form pores. In addition, our simulations show that fibril-like structures produce little damage to lipid membranes, as non-polar side chains in these structures are unavailable to interact with the acyl tail of lipids.

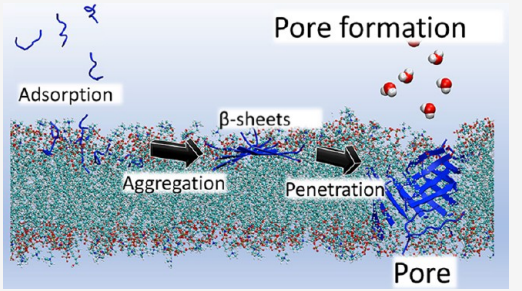

KEYWORDS: *amyloid, lipid membrane, membrane damage, poration, detergent-like effect*

INTRODUCTION

Several amphipathic peptides are toxic and can cause cell death. They comprise amyloid peptides related to neurodegenerative diseases,[1−3] antimicrobial peptides that enable organisms to defend themselves against biological threats,[4−6] and artificially designed peptides.[7,8] Extensive studies have been dedicated to provide insights into the mechanisms accounting for their toxicity, which include non-specific interactions with the cell membrane. These interactions enable lipids to be extracted from the bilayer (i.e., detergent-like mechanism of membrane damage) and ions to permeate the membrane via the formation of pore-like structures in its surface.[9−19] An understanding of the pathways and interactions required to account for these types of membrane damage is critical to enable the development of therapeutics for amyloid diseases and to guide the design of novel antimicrobial peptides.[20,21]

Computer simulations have the potential to provide important new atomic insights into our understanding of membrane damage by amphipathic peptides.[18,22,23] However, all-atom simulations of peptide aggregation on the membrane surface and their penetration into the lipid bilayer are computationally demanding. Accordingly, the spontaneous formation of pores has only been simulated for α-helical peptides, which retain their secondary structure in the non-polar environment of the bilayer, where intrapeptide hydrogen bonds are more stable than in solution.[23] These unbiased simulations have been performed at high temperatures to allow peptides to penetrate the bilayer in a time-scale accessible to supercomputers (>5 μs). The early stages of melittin aggregation have been captured by these simulations showing that this peptide forms transient pores in the bilayer.[24−26] Attempts to simulate the spontaneous formation of pore-like structures by β-sheet peptides have not been successful so far. For example, low-molecular-weight oligomers from amyloid peptides[27−30] as well as β-sheets made from up to eight antimicrobial protegrin-1 peptides[31] did not penetrate the membrane in long all-atom simulations.

Evidence that membrane damage by amyloids and β-hairpin peptides can involve the formation of pores is provided by atomic force microscopy, wherein the radius of pores is reported to be 1−2 nm.[32−34] Computationally, pore-like damages are often studied starting with peptides already inserted in the interior of the membrane to reduce the time-

Received: July 27, 2022
Accepted: August 31, 2022
Published: September 12, 2022

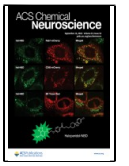

https://doi.org/10.1021/acschemneuro.2c00446
ACS Chem. Neurosci. 2022, 13, 2766−2777

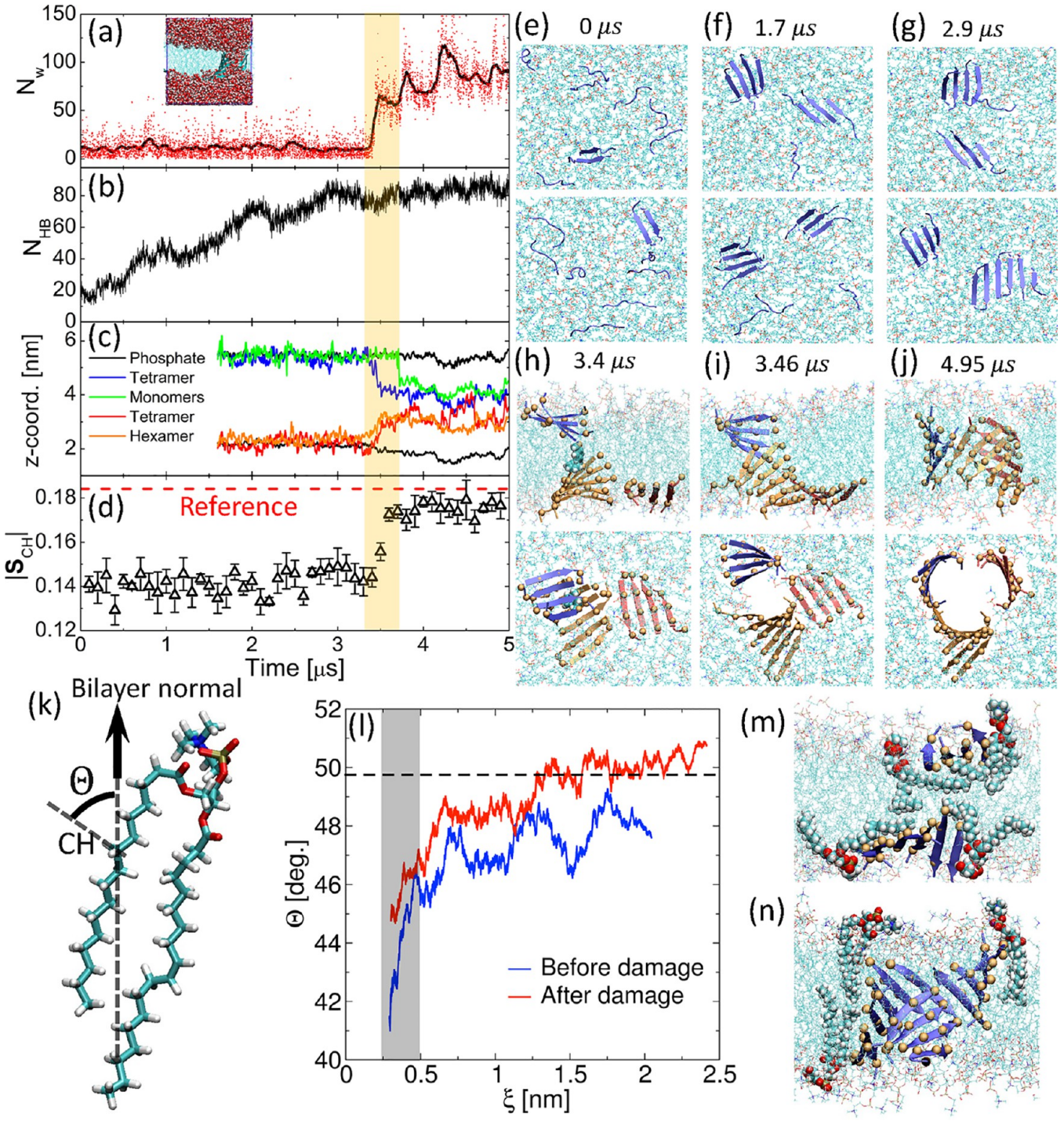

Figure 1. Spontaneous formation of pores starting with peptides on both membrane leaflets. (a) Number N_w of water molecules in the dry core of the bilayer (red dots) and its 100 point moving average (black line). The inset highlights water permeation at 3.78 μs. (b) Number N_{HB} of interbackbone hydrogen bonds. (c) z-Position of the COM of the different β-sheets and POPC phosphate atoms. (d) Order parameter $|S_{CH}|$ computed for the methylene group of the sixth carbon atoms of POPC/POPG acyl chains. The red dashed line corresponds to the reference $|S_{CH}|$ computed for a bilayer simulated without peptides. (e–j) Visual representation of peptides (in blue) on the bilayer at different times. For panels e–g, upper and lower snapshots correspond to views of top and bottom leaflets of the bilayer. For panels h–j, upper and lower snapshots correspond to views of the cross section and top leaflet of the bilayer. For the latter panels, α-carbon atoms of phenylalanine residues are represented by orange beads. (k) Definition of the angle Θ used to define $|S_{CH}|$. (l) Dependence of Θ on the minimal distance ξ of lipids to peptides. Visual representations of lipid when β-sheets are (m) deposited on the membrane and (n) forming pores.

cost to simulate their aggregation and penetration in the bilayer.[35−45] Accordingly, idealized pores from amyloid and β-hairpin antimicrobial peptides have been shown to be stable in all-atom simulations although they perturb lipids inside the bilayer.[31,46−50] In addition to pore formation, experimental studies have shown that amyloids and β-hairpin antimicrobial peptides can also cause damage by removing lipids from the membrane surface.[10−14] These phenomena have been related

https://doi.org/10.1021/acschemneuro.2c00446
ACS Chem. Neurosci. 2022, 13, 2766−2777

to the amphipathic nature of these peptides that can bind simultaneously non-polar and polar moieties of lipids as well as solvent molecules.[51−54] Despite these insights, the sequence of events and the interactions accounting for both the removal of lipids from the bilayer and poration[55,56] by amyloids and β-hairpin peptides remain mostly unknown.

In this paper, we study membrane damage by a short amphipathic peptide with sequence alternating between non-polar and charged residues: Ac-$(FKFE)_2$-NH_2. This peptide self-assembles promptly into amyloid-like fibrils in solution making it suitable for computational studies.[57−59] Moreover, it was shown to bind strongly to lipid bilayers.[60] Here, all-atom simulations are used to study the sequence of events accounting for the self-assembly of membrane-bound Ac-$(FKFE)_2$-NH_2 peptides into β-sheets that spontaneously penetrate the membrane to form pore-like structures. The spontaneous removal of lipids from model membranes by Ac-$(FKFE)_2$-NH_2 peptides are also simulated providing one of the first atomic insights into this type of membrane damage. An analysis of these simulations shows that interactions of lipid tails with non-polar side chains play an important role in accounting for membrane damage. They enable lipids to be dragged out of the bilayer and contribute to stabilize pore-like structures.

In our simulations, lipid removal takes place during the interaction of two membrane-bound β-sheets as they emerge out of the membrane to bury their non-polar residues against each other. In this process, lipids that are strongly bound to non-polar residues are dragged out of the membrane. We find that membrane-bound β-sheets become twisted during the simulations with one of their extremities partially penetrating the core of the bilayer. This partial penetration allowed peptides on opposite leaflets to interact and form a long transmembrane β-sheet initiating poration. The twist in β-sheets also allows water molecules to partially penetrate the membrane. In simulations where peptides are deposited on a single membrane leaflet, two β-sheets penetrate the membrane by tilting their polar faces toward these water molecules. This takes place while their non-polar residues remain bound to the acyl tail of lipids leading to the formation of pores with diameters ranging from 1.2 to 1.8 nm. Charged and non-polar residues of these β-sheets face the interior and exterior of pores, respectively. We also show that fibril-like structures do not perturb the membrane significantly in our simulations.

RESULTS AND DISCUSSION

Pore-like Membrane Damage. *Peptides Deposited on Both Membrane Leaflets.* Three 5 μs simulations were performed with 18 peptides randomly deposited on both leaflets of a 7:3 POPC/POPG bilayer made with 128 lipids. A temperature of 350 K was used to accelerate diffusion enabling the formation of small-size β-sheets within a time-frame of ∼3 μs. In two of the three simulations performed here, β-sheets interacted with each other leading to the formation of a pore in the lipid membrane. These phenomena are characterized in Figure 1 for one of the simulations. In this figure, panel a shows number N_w of water molecules in the space between the two leaflets. This quantity is mostly zero in the beginning of the simulation and it increases abruptly close to 3.4 μs when poration takes place. The inset of this panel shows water molecules permeating the membrane at the end of the simulation. Panel b quantifies peptide aggregation by showing the number of backbone hydrogen bonds as a function of time. This quantity increases as peptides encounter each other on the membrane surface forming small-size β-sheets.[58,61,62] Panels e−g illustrate this aggregation process through snapshots of peptides on upper (top panels) and lower (bottom panels) leaflets at different instances of time. Panel e depicts isolated peptides and dimers at the beginning of the simulation. At 1.7 μs (panel f), aggregation leads to the formation of trimers and tetramers on both membrane leaflets. At ∼2.9 μs, the number of hydrogen bonds saturates (see panel b) and the larger aggregates that have formed are hexamer and tetramer on one leaflet and tetramer and dimer on the other—see panel g. The formation of tetramers or larger β-sheets preceded poration in all simulations where this phenomenon took place.

Panel c shows the position of the center-of-mass (COM) of the different β-sheets along the direction normal to the membrane surface, that is, z-axis. In this panel, the position of maximum density of POPC phosphate atoms is also shown as a reference. Peptides remain on the surface of the bilayer until very close to poration, when hexamer (in orange) and tetramer (in blue) on bottom and top leaflets, respectively, penetrate the membrane. Penetration takes places within the short-time window (i.e., ∼0.2 μs) highlighted by the shaded area in Figure 1. Subsequently, tetramer (in red) and monomers (in green) penetrate the bilayer from bottom and upper leaflets, respectively. Poration starts when some of the atoms of β-sheets that are on opposite leaflets (i.e., hexamer and tetramer) hover on top of each other—see panel h. These atoms are the first to penetrate the membrane causing β-sheets to twist—see panel h−i. This enables peptides on opposite leaflets to interact with each other half way along the bilayer cross section to create a long transmembrane β-sheet made of 10 peptides—see panel j. The latter accounts for half of the surface of a cylindrical pore inside the membrane. The other half of the cylindrical pore is formed by the tetramer from the bottom leaflet. Peptides forming the cylinder have non-polar and charged side chains facing its exterior and interior, respectively.[20] Moreover, the diameter of the cross section of the pore that is available to the solvent is approximately 1.77 nm.

Notice that the spontaneous formation of a stable pore implies that the assembly of β-sheets in a cylindrical structure inside the bilayer is more favorable energetically than having individual β-sheets dispersed on the membrane surface. We hypothesize that a reduction in the distortions of acyl tail of lipids contributes to favor these pore-like assemblies of β-sheets. This is investigated in panel d, where the magnitude of the deuterium order parameter is shown as a function of time. This quantity is defined as $|\mathbf{S}_{CH}| = \left\langle \left| \frac{3\cos^2\Theta - 1}{2} \right| \right\rangle$, where Θ is the angle between carbon−hydrogen bonds of methylene groups and the bilayer normal[63,64]—see panel k. In Figure S6, we show $|\mathbf{S}_{CH}|$ computed for all carbon atoms for the different lipid tails used in our simulations at 350 and 320 K. For clarity, panel d shows $|\mathbf{S}_{CH}|$ computed for the methylene group of the sixth POPC carbon atom averaged over all lipids in the simulation box and all conformations within a time frame of 0.1 μs. Errors were estimated using block average, wherein the 0.1 μs trajectory were divided into blocks spanning 0.02 μs in time. As a reference, $|\mathbf{S}_{CH}|$ computed for a 7:3 POPC/POPG bilayer simulated without peptides is shown as a red dotted line in panel d. Before pore formation, $|\mathbf{S}_{CH}|$ deviates significantly from the reference bilayer suggesting strong

https://doi.org/10.1021/acschemneuro.2c00446
ACS Chem. Neurosci. 2022, 13, 2766−2777

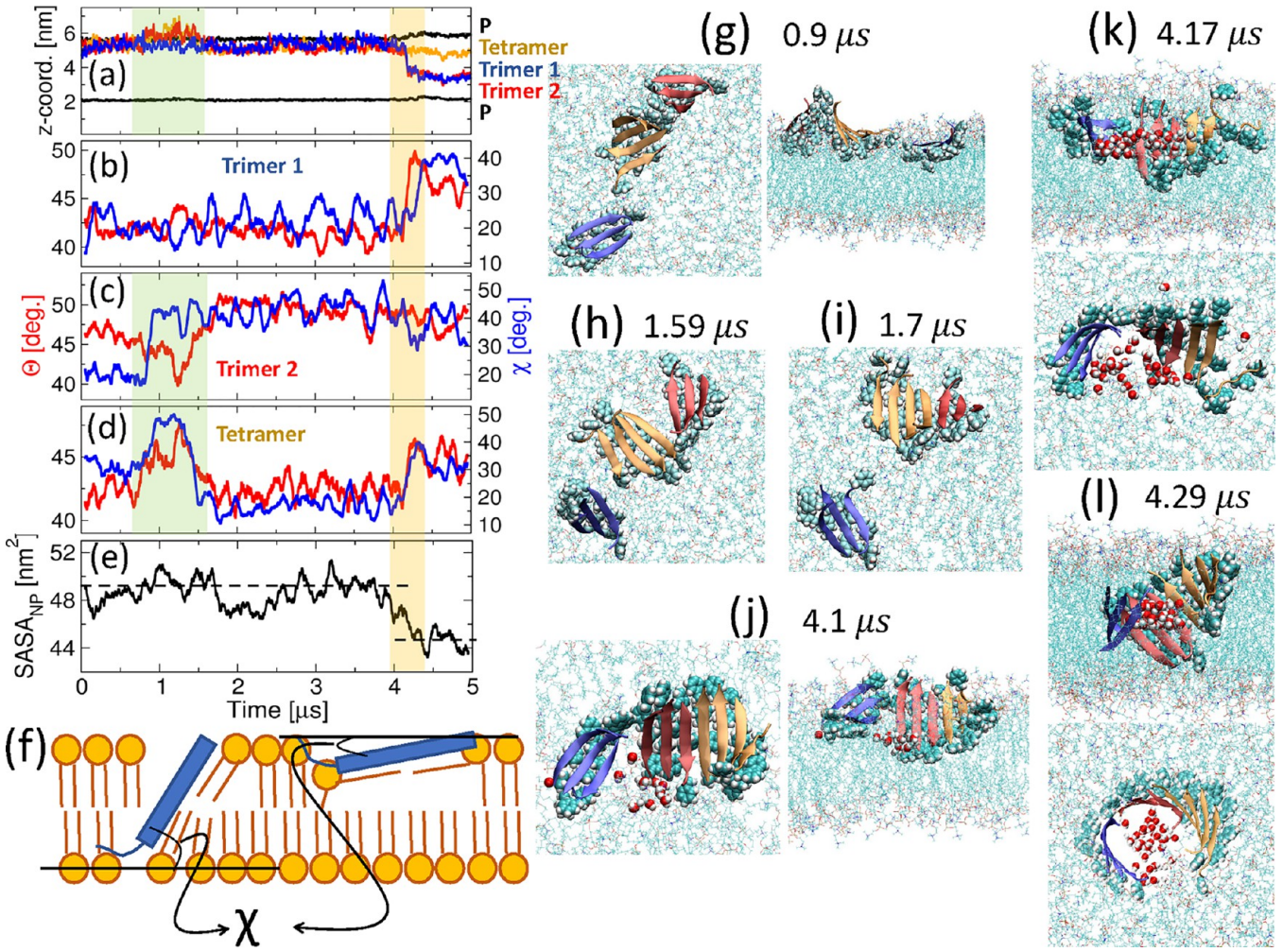

Figure 2. Pore formation by β-sheets deposited on one of the membrane leaflets. (a) z-Coordinate of the COM of the different β-sheets and DPPC phosphate atoms (in black). Time dependence of Θ (in red) and χ (in blue) computed for (b) trimer 1, (c) trimer 2, and (d) tetramer. (e) Solvent accessible surface area of non-polar moieties (i.e., $SASA_{NP}$) of both peptides and lipids. Average values of $SASA_{NP}$ computed before and after poration are shown using black dashed lines. (f) Schematic representation of angle χ for two β-sheets represented in blue. (g–l) Visual representations of β-sheets on the membrane surface at times. A view from the top of the membrane is provided for all time frames. A cross-sectional view of the membrane is also shown in panels g and j–l. β-Sheets are represented using the same color code as in panel a. Atoms of phenylalanine side chains are represented using a van der Waals representation. Only water molecules that penetrate deeply within the bilayer are shown in panels j–l.

distortions in lipid tails. The formation of a pore leads to a reduction in these distortions as $|S_{CH}|$ approaches the reference value. Order parameters for other methylene groups of POPC (not shown here) exhibit a similar abrupt change in $|S_{CH}|$ when a pore is formed.

Panel l provides insights into lipid tail conformations by depicting average angle Θ of lipids as a function of their minimal distance ξ from peptides. This distance is computed between phosphate atoms of lipid head groups and Cα atoms of peptides. Red and blue lines correspond to Θ computed just before (2.9–3.0 μs) and just after (3.1–3.2 μs) pore formation, respectively. This panel shows that close to peptide (highlighted by the gray area in the figure) lipid tails are more parallel to the membrane surface (i.e., Θ is smaller) before poration compared to after poration. This can be explained by favorable interactions between atoms of lipid tails and non-polar side chains. These interactions, which hold peptides anchored on the membrane surface,[60,65] also induce distortions in the lipid tail as depicted in panel m. The latter panel highlights selected lipids that are close to β-sheets before poration. Notice that acyl tails of those lipids are almost parallel to the membrane surface filling the void in the bilayer beneath β-sheets[66] and maximizing their interactions with phenylalanine side chains. Panel n highlights lipids that are close to the cylindrical pore. Hydrophobic tails of those lipids are oriented perpendicularly to the membrane surface maximizing their interactions with phenylalanine side chains of pore structures.

In addition to Figure 1, results from an independent 5 μs simulation performed at 350 K and starting with 18 peptides deposited on both membrane leaflets of a 7:3 POPC/POPG bilayer are shown in Figure S1. Also, in an attempt to study poration at a lower temperature, we reduced the temperature of the trajectory as shown in Figure 1 to 320 K when it reached 2.5 μs, that is, ∼1 μs before poration. At this instant, the monomers had already aggregated into small β-sheets without penetrating into the bilayer. This system was simulated for 4 μs, as shown in Figure S2. Both of these additional simulations are characterized by large distortions in the orientation of lipid tails due to the presence of β-sheets on the membrane surface.

https://doi.org/10.1021/acschemneuro.2c00446
ACS Chem. Neurosci. 2022, 13, 2766–2777

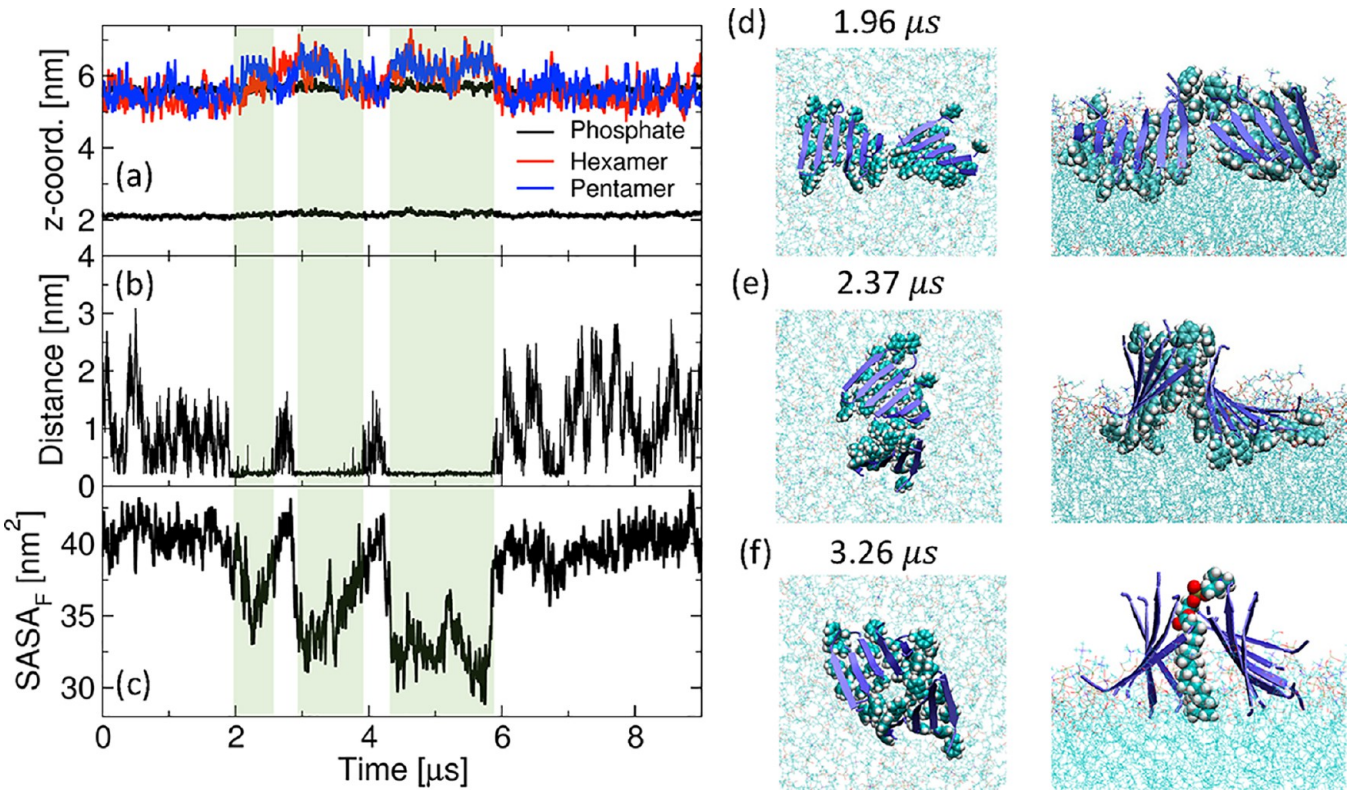

Figure 3. Detergent-like damage starting with β-sheets deposited on the membrane surface. (a) z-Coordinate of the COM of β-sheets and POPC phosphate atoms. (b) Minimal distance between the hexamer and pentamer. The three shaded areas in panels a−c highlight regions in which β-sheets emerge out of the membrane surface. (c) Solvent accessible surface area (SASA$_F$) of phenylalanine side chains assuming that there is no lipids in the solutions. (d−f) Visual representation of β-sheets (in blue) on the bilayer at (d) 1.96, (e) 2.37, and (f) 3.26 μs. Atoms of phenylalanine side chains are highlighted using a van der Waals representation. Left and right panels correspond to top and cross-section views of the bilayer. A selected lipid emerging out of the membrane is highlighted in panel f.

These distortions are significantly reduced during pore formation. Moreover, in these simulations, poration started with peptides on opposite leaflets penetrating the bilayer to interact with each other, which is consistent with results from Figure 1. Notice that there is increasing evidence that the Aβ peptide related to Alzheimer's disease can be found both in the intracellular as well as in the extracellular space.[67−69] This may give rise to a scenario where poration emerges from the interaction of peptides on opposite leaflets of the bilayer, as shown in Figure 1. However, in vitro studies have also reported pore formation from peptides on just one leaflet of the bilayer. This situation is studied below.

β-Sheets Deposited on Just One Membrane Leaflet. Poration was observed in a simulation, where two trimers and one tetramer, were deposited on the same leaflet of a 7:3 DPPC/DPPG bilayer at 350 K. In this simulation, the tetramer and one of the trimers interacted to form a heptamer at 1 μs. This was followed by poration at 4.2 μs when interactions between the heptamer and the remaining trimer on the membrane led to the formation of a cylinder inside the bilayer. These events are characterized in Figure 2, where panel a shows the z-coordinate of the COM of the different β-sheets, and panels b-d depict angle χ formed between the surface of β-sheets and the membrane surface—see schematic representation in Figure 2f. In panels b−d, angle Θ characterizing the orientation of lipid tails (see definition in Figure 1k) in the vicinity of these sheets is also shown. We considered a lipid to be in the vicinity of a β-sheet if the minimum atomic distance of their tails to phenylalanine residues is smaller than 0.5 nm.

Heptamer formation and poration account for large changes in χ, Θ, and the z-coordinate of the β-sheets involved in these phenomena as highlighted by green and orange areas in Figure 2a−d, respectively. Heptamer formation starts with the interaction between phenylalanine side chains at the edges of the tetramer and one of the trimers, as depicted in panel g. These β-sheets partially emerge out of the membrane surface enabling their non-polar faces to pack against each other to maximize favorable interactions between phenylalanine residues—see panel g. Accordingly, the z-coordinate of the COM of these β-sheets within the highlighted green area in panel a emerges out of the bilayer boundary given by phosphate atoms. This is characterized by an increase in χ in panels c,d. These β-sheet conformations remain stable for more than 0.5 μs (see green area) after which trimer and tetramer approaches each other in an orientation that allows their backbone atoms to hydrogen bond—see panel h. This accounts for the formation of a stable β-sheet made from seven peptides in panel i. Until poration takes place, this larger β-sheet remains twisted with one of its extremities being mostly parallel to the membrane surface (i.e., $\chi \sim 15°$ in panel d) and the other extremity being tilted (i.e., $\chi \sim 40°$ in panel c). This correlates with the orientation of lipid tails, which are more parallel to the membrane surface (i.e., $\Theta \sim 40°$ in panel d) around the former β-sheet extremity than around the latter extremity (i.e., $\Theta \sim 50°$ in panel c). As in Figure 1, this correlation can be related to interactions between non-polar side chains and lipid tails.

Poration is preceded by the partial penetration of water molecules, which are attracted to the charged face of β-sheets,

https://doi.org/10.1021/acschemneuro.2c00446
ACS Chem. Neurosci. 2022, 13, 2766−2777

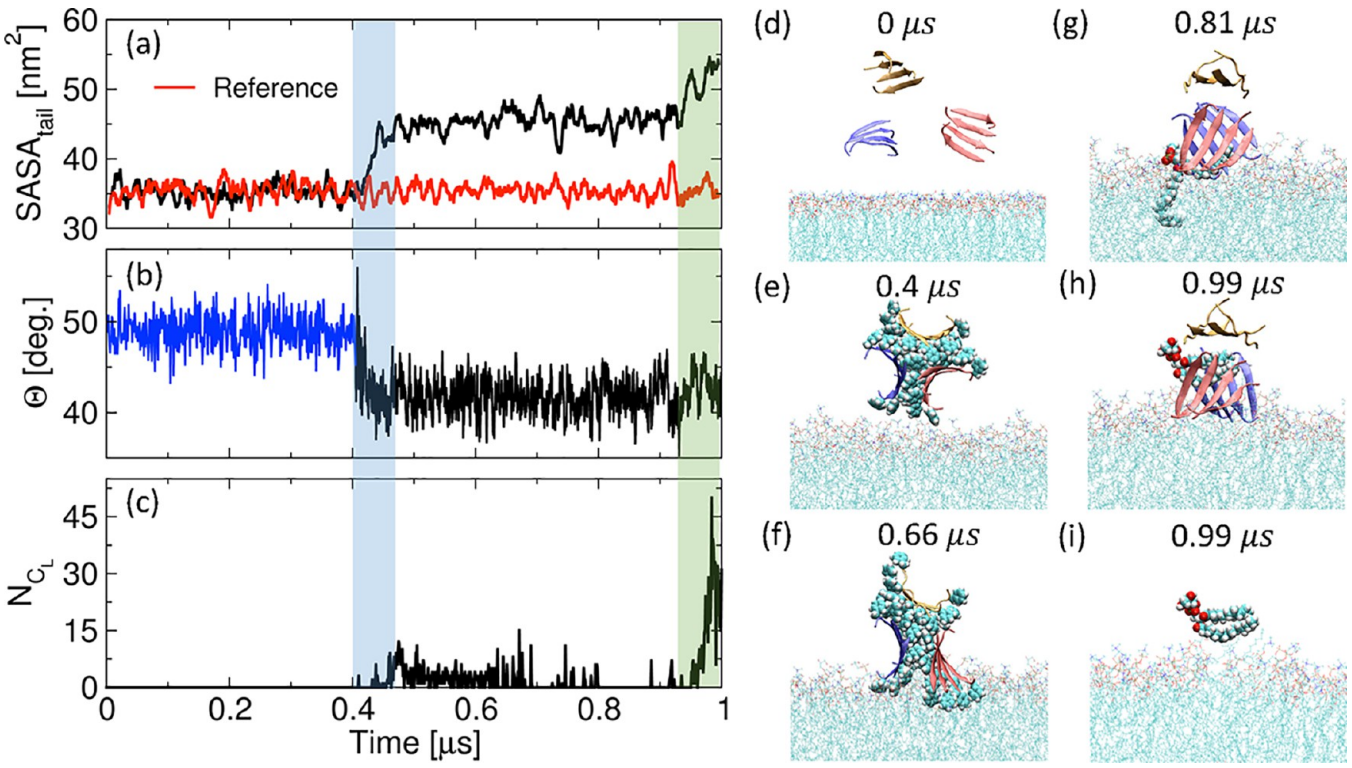

Figure 4. Detergent-like damage starting with β-sheets in solution. (a) Solvent accessible surface area of lipid tail atoms, that is, SASA$_{tail}$, assuming peptides are not in the simulation box. (b) Angle Θ computed for lipids that are in the vicinity of β-sheets. Cut-offs of 3.0 nm (blue line) and 0.5 nm (black line) are used to compute lipids in the vicinity of β-sheets before and after peptides bind to the membrane. (c) Number of lipid tail carbon atoms with z-coordinate outside the boundary given by the average position of nitrogen atoms of lipid head groups of upper and lower leaflets. (d−h) Visual representations of β-sheets on the lipid bilayer at different time intervals. A lipid emerging out of the bilayer is highlighted in panels g−h. Panel i highlights this lipid by hiding the trilobal structure.

inside the membrane. As illustrated in panel j, this penetration is pronounced around the twisted extremity of the heptamer (i.e., red β-sheet) when it interacts with the remaining trimer (blue β-sheet) on the membrane. This causes polar faces of β-sheets to wrap themselves around these water molecules to reduce the accessibility of non-polar groups of the bilayer to the solvent, as shown in panels k,l. Accordingly, the solvent accessible surface area (SASA$_{NP}$) of non-polar groups decreases during poration as shown in panel e. This minimizes unfavorable interactions of water with non-polar lipid tails inside the membrane and it contributes to stabilize the cylindrical pore structure.

In summary, small-size oligomers on the membrane surface can interact with each other via the formation of contacts between non-polar side chains. This can trigger β-sheets to bury their non-polar side chains against each leading them to partially emerge from the membrane surface—see panel g. Alternatively, backbone atoms of β-sheets that are brought close to each other may form hydrogen bonds accounting for a longer β-sheet—see panel h−i. The latter becomes twisted on the membrane wherein one of its extremities remains parallel to the surface and the other penetrates the membrane—see panel j. Together with the latter extremity, water molecules, which are attracted to polar faces of β-sheets, partially penetrate inside the membrane surface—see panel j. This unfavorable presence of water inside the bilayer is minimized by tilting the polar face of β-sheets toward the axis where solvent molecules are located—panel k. This, combined with a reduction in lipid tail distortions accounts for the formation and stabilization of pore-like structures enabling water molecules to permeate membranes. The diameter of the cross section of the cylindrical pore available to the solvent in panel l is approximately 1.24 nm.

In addition to Figure 2, poration from just one membrane leaflet was also simulated using a 7:3 DMPC/DMPG bilayer at 350 and 320 K—see Figures S3 and S4. This phenomenon required only 3 μs to take place in this thinner bilayer compared to the DPPC/DPPG membrane shown in Figure 2. In both of these simulations, poration accounted for a significant reduction in lipid tail distortions, and, before poration, β-sheets were twisted. This is consistent with results from Figure 2. Simulations starting with β-sheets on just one membrane leaflet were also performed using a 7:3 POPC/POPG bilayer at 350 K. This simulation did, however, not form a pore even after 9 μs and it is discussed in the next section.

Detergent-like Damage. Figure 3 characterizes the trajectory of a 9 μs simulation, wherein hexamer and pentamer β-sheets are deposited on one leaflet of a 7:3 POPC/POPG bilayer at 350 K. In this simulation, hexamer and pentamer do not penetrate the bilayer nor do they hydrogen bond with each other to form a larger β-sheet. Instead, these oligomers partially emerge out of the lipid bilayer at three occasions similarly to the events preceding heptamer formation in Figure 2. These attempts to leave the membrane are highlighted by green shaded areas in Figure 3a, where z-coordinates of the COM of hexamer and pentamer are found outside the region delimited by phosphate atoms on both leaflets. Panel b depicts the minimum distance between the hexamer and pentamer. It shows that attempts of β-sheets to emerge out of the bilayer

https://doi.org/10.1021/acschemneuro.2c00446
ACS Chem. Neurosci. 2022, 13, 2766−2777

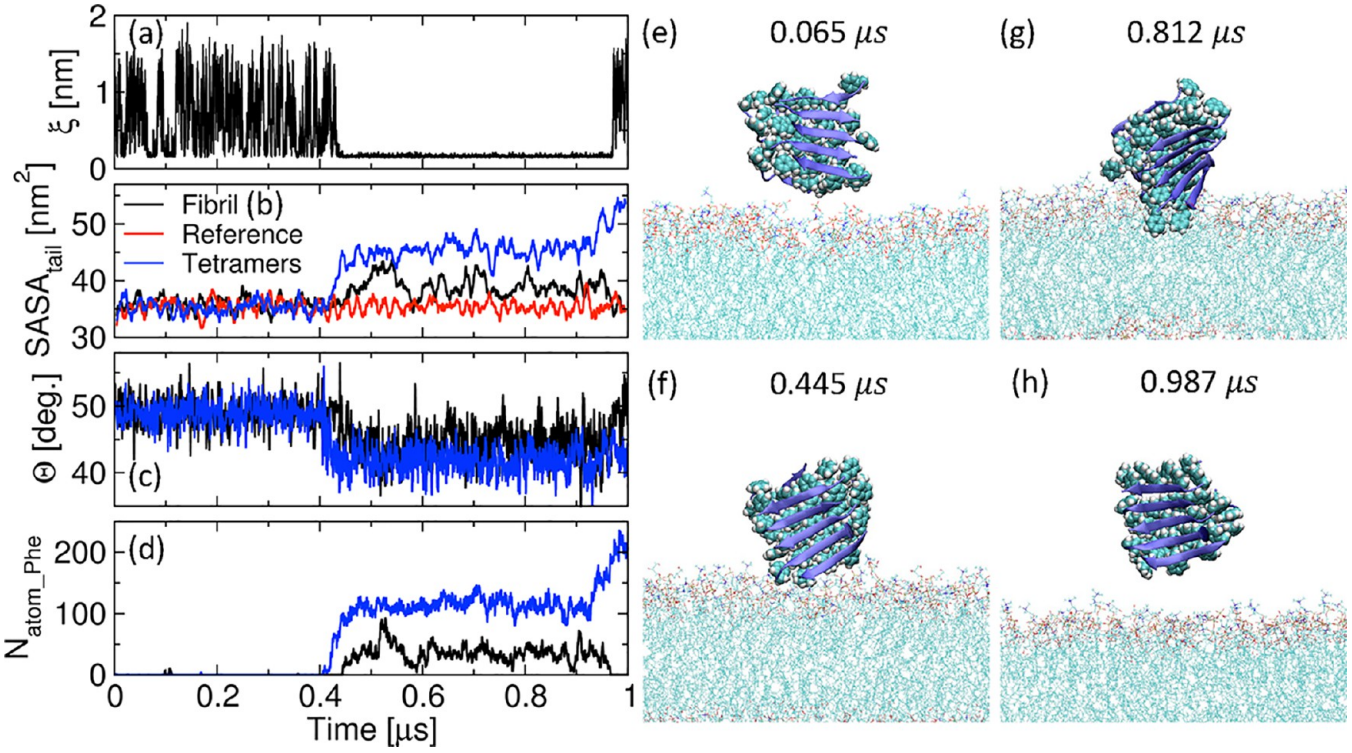

Figure 5. Fibrils do not damage lipid membranes significantly. (a) Minimal distance ξ between atoms of the fibril and the bilayer. (b) Contribution of lipid tail atoms to the solvent accessible surface area of the bilayer (i.e., $SASA_{tail}$) assuming that peptides are not in the simulation box. Black, blue, and red lines are for simulations performed with a fibril in the solution, the trilobal structure of Figuer 4, and no peptides. (c) Average angle Θ of lipids that are in the vicinity of a fibril (in black) or of the trilobal structure of Figure 4 (in blue). As in Figure 4, two cut-offs (3.0 or 0.5 nm) were used to determine lipids that are in the vicinity of peptides. The larger cut-off was used when peptides were in the solution before interacting with lipids. The shorter cut-off was used when peptides were interacting with the bilayer. (d) Number of phenylalanine side-chain atoms that are at a distance smaller than 0.5 nm from lipid tails. Black and blue lines are for simulations performed with a fibril and trilobal structure, respectively. (e–h) Visual representations of fibril and bilayer at different instants of time. A van der Waals representation is used for phenylalanine side chain.

only take place when they are interacting with each other, that is, their distance is minimal. As in the case of heptamer formation in Figure 2, the force driving these events is the packing of phenylalanine side chains of different β-sheets against each other. These interactions are maximized when non-polar faces of the hexamer and pentamer are buried against each other instead of facing the dry core of the bilayer. Packing of phenylalanine side chains is quantified in panel c, where the solvent accessible surface area of phenylalanine side chains ($SASA_F$) is computed assuming that there is no lipids in the solutions. As the hexamer and pentamer emerge out of the lipid membrane, phenylalanine side chains become buried against each other and $SASA_F$ decreases. Conversely, $SASA_F$ is maximum when these β-sheets are deposited flat on the membrane.

Selected conformations of β-sheets as they emerge out the membrane are shown in panels d–f. These events take place when phenylalanine side chains at the edge of the hexamer and pentamer interact with each other. During the first attempt to emerge out of the membrane, only a few side chains are interacting with each other—see panel d. During the second attempt, edges of hexamer and pentamer are better aligned enabling more phenylalanine side chains to interact—see panel e. These interactions are optimized in the third attempt to emerge out of the membrane—see panel f. Accordingly, the magnitude of $SASA_F$ in panel c drops to its lowest value in third, followed by second, and first attempts to leave the membrane. This accounts for the greater stability of the third event that survives for almost 2 μs, whereas the second and first events last for slightly more and less than 1 μs, respectively. In the third attempt to emerge out of the membrane, a lipid trapped in between the hexamer and pentamer emerges out of the membrane—see panel f. In this configuration, lipid head and tails are exposed to the solvent and buried in between non-polar faces of β-sheets, respectively. This illustrates how the amphipathic nature of β-sheets can behave as a "detergent" removing lipids from the core of the bilayer.

The removal of lipids from the bilayer can also take place starting with β-sheets in the solution. This is illustrated in Figure 4 for a simulation performed with three tetramers initially located randomly in the solution—see panel d. Hydrophobic interactions between phenylalanine side chains drive tetramers towards each other enabling the formation of the *trilobal* structure in panel e. This is followed closely by the interaction of this aggregate with the 7:3 POPC/POPG membrane depicted in panel f. Favorable interactions between lipid tails and phenylalanine side chains stabilize the trilobal structure onto the surface of the bilayer wherein lipid tail atoms are attracted to the dry core of the trilobal structure.

To provide insights into the integrity of the membrane, Figure 4a shows contributions of lipid tail atoms to the solvent accessible surface area ($SASA_{tail}$) of the bilayer in the absence of peptides. This quantity is a minimum when the bilayer is unperturbed with all lipid tails packed in the dry membrane core, and it increases when lipid tails become exposed at the

https://doi.org/10.1021/acschemneuro.2c00446
ACS Chem. Neurosci. 2022, 13, 2766–2777

bilayer surface. As a reference, we show results for a simulation performed without tetramers (see red line) wherein $SASA_{tail}$ fluctuates around 35 nm^2 during the whole simulation. Before binding of the trilobal structure to the membrane surface, $SASA_{tail}$ also fluctuates around 35 nm^2. However, this quantity increases abruptly at ∼0.4 μs when the trilobal structure anchors onto the membrane causing lipid tails to become exposed at the membrane−protein interface. This exposure can be quantified by computing the angle Θ (defined in Figure 1k), which characterizes the orientation of lipid tails that are in the vicinity of the trilobal structure. As in Figure 2b−d, we consider a lipid to be in the vicinity of a β-sheet if the minimum atomic distance of their lipid tails to phenylalanine residues is smaller than the cut-off distance of 0.5 nm—see black line in panel b. Since there are no lipids in the vicinity of β-sheets in the beginning of the simulation (i.e., <0.4 μs), Θ was estimated using the larger cut-off distance of 3.0 nm—see blue line in panel b. Using the latter definition, Θ fluctuates around 50°, which is consistent with the orientation of lipid tails away from pore structures in Figure 1j, where damage is minimal. As soon as the trilobal structure binds to the membrane (see blue shaded area in Figure 2a−c), the value of Θ drops abruptly to approximately 40°. This highlights the tendency of lipid tails to become more parallel to the membrane surface close to the trilobal structure as illustrated in panel g.

Close to the end of the simulation (shaded green area in Figure 4a−c), some lipids are almost completely removed from the membrane surface wherein their interactions with phenylalanine side chains are maximized—see panels h−i. As in Figure 3f, this highlights the potential of amphipathic β-sheets to dismantle the membrane via a detergent-like mechanisms where lipids are dragged out of the bilayer. This is quantified in Figure 4c by computing the number of lipid tails carbon atoms N_{C_L} with z-coordinate outside the boundary given by nitrogen atoms of lipid head groups of upper and lower leaflets. Panel c shows that a small number of lipid tail atoms emerge out of the membrane soon after the trilobal structure starts interacting with the bilayer. This number increases abruptly close to the end of the simulations characterizing the removal of lipids as depicted in panels h−i.

Note that a trilobal structure was formed in the four trajectories we generated with three tetramers in the solution. In all of these trajectories, the interactions of the trilobal structure with the membrane accounted for lipid removal. This is illustrated for another trajectory in Figure S5. It highlights the robustness of the detergent-like mechanism of membrane damage by amyloid-like peptides, which has been reported experimentally for different amyloid proteins.[10,52,53]

Fibrils Are Less Toxic. Figure 5 characterizes the interaction of a small fibril with a 7:3 POPC/POPG bilayer at 350 K. The fibril is assembled by packing non-polar faces of two anti-parallel β-sheets made from five Ac-$(FKFE)_2$-NH_2 peptides each. Panel a shows the time evolution of the minimum distance between the fibril and bilayer. The fibril undergoes several binding−unbinding events during the first 0.4 μs after which it remains bound to the bilayer surface until very close to the end of the simulation when it becomes detached. Panel b shows contributions of lipid tails to the solvent accessible surface area of the bilayer in the absence of the fibril, that is, $SASA_{tail}$. As a comparison, $SASA_{tail}$ is also shown for both a bilayer unperturbed by peptides (in red) and the bilayer interacting with the *trilobal* structure in Figure 4 (in blue). This figure shows that interactions of the fibril with the bilayer increases the exposure of lipid tails when compared to simulations performed without peptides. This exposure is, however, significantly lower than the one caused by the trilobal structure. Panel c depicts average angle Θ of lipid tail in the vicinity of the fibril (in black) and the *trilobal* structure (in blue). As in Figure 4, a lipid is considered to be in the vicinity of the fibril if the minimum atomic distance of its acyl tails to phenylalanine residues is smaller than a cut-off distance of 0.5 nm. A larger cut-off distance of 3.0 nm is used in the beginning of the simulation when the fibril is not in contact with the bilayer. This panel shows that interactions of the fibril or the *trilobal* structure with the bilayer account for a reduction in Θ as the acyl tail of lipids become more distorted. The latter distortions are, however, less pronounced around the fibril than around the *trilobal* structure. These differences can be related to less pronounced interactions between phenylalanine side chains and the lipid bilayer. Accordingly, panel g and Figure 4f depict two and at least four phenylalanine side chains deeply buried inside the bilayer for the fibril and *trilobal* structure, respectively. This is quantified in panel d where the number of phenylalanine side-chain atoms that are at a distance smaller than 0.5 nm from any lipid tail is shown. These numbers are higher for the *trilobal* structure than for the fibril. Thus, although our simulations cannot assert that fibrils are non-toxic due to the limited simulation time, it disrupts the membrane less significantly than oligomers/trilobal structures. At the end of the simulation (i.e., panel h), the fibril detaches itself from the membrane.

CONCLUSIONS

The atomic details of how amyloids and β-hairpin peptides interact with lipid membranes causing damage remains unclear. This knowledge is critical to develop new treatments for amyloid diseases as well as to rationally design antimicrobial peptides. Here, we performed one of the first all-atom simulations in which membrane-bound peptides self-assemble into β-sheets that subsequently either form pores on the membrane surface or drag lipids out of the bilayer core. An analysis of these simulations shows that these mechanisms of membrane damage are strongly affected by interactions between non-polar side chains and the acyl tail of lipids, which hold peptides anchored onto the membrane surface.[60] These strong interactions enable lipids to be dragged out of the bilayer by oligomeric structures in a detergent-like manner. They also account for distortions in the orientation of lipid tails that are minimized when pores are formed.

In our simulations, membrane damage took place as a result of the interaction between two β-sheets. In detergent-like damages, two β-sheets emerge out of the membrane to bury their non-polar residues against each other. In this process, lipid tails that are strongly bound to non-polar residues are also dragged out of the membrane. In pore-like damages, two β-sheets penetrate the membrane while maintaining their non-polar residues buried against the dry core of the bilayer. Each β-sheet accounts for half of the cylindrical surface of pores that have diameters ranging from 1.2 to 1.8 nm in our simulations. Notice that non-polar residues are buried in the dry core of fibrils and, thus, these structures did not perturb lipid membranes in a significant manner in our simulations.

In simulations, membrane-bound β-sheets become twisted with one of their extremities partially penetrating the lipid

https://doi.org/10.1021/acschemneuro.2c00446
ACS Chem. Neurosci. 2022, 13, 2766−2777

bilayer. This allows peptides on opposite leaflets to interact and form long transmembrane β-sheets that initiate poration. The twist of β-sheets also allows water molecules to partially penetrate the membrane. In simulations where peptides are deposited on a single leaflet, β-sheets penetrate the membrane by tilting their polar faces toward these partially penetrating water molecules while keeping non-polar residues buried against acyl-tails of lipids.

The mechanistic insights brought up by this study were obtained from an analysis of several simulations (a total of ~40 μs) performed at two temperatures (320 or 350 K), using three anionic membranes, and different numbers of peptides on the membrane/solution. The results obtained from this study are, therefore, robust but their scope needs to be tested for other peptide sequences. We also believe that important new insights will be obtained by simulating membrane damage using different lipid compositions, which has been shown to affect the onset of amyloid diseases.[1,70−74]

METHODOLOGY

Molecular Dynamics Simulation. Amphipathic peptides with sequence that alternates strictly between non-polar (i.e., phenylalanine F) and charged amino acids (i.e., positive lysine K, and negative glutamic acid E), that is, Ac-$(FKFE)_2$-NH_2, is used to study membrane damage. Experimental studies have shown that this peptide self-assembles into amyloid fibrils forming supramolecular nanotubes.[57,59,75] In all-atom simulations, this peptide was also shown to self-assemble into amyloid-like fibrils and to interact with lipid membranes in a computationally accessible time-frame.[58,60] Here, membrane damage is studied using three anionic membranes made by combining zwitterionic, that is, 1-palmitoyl-2-oleoyl-*sn*-glycero-3-phosphocholine (POPC), 1,2-dipalmitoyl-*sn*-glycero-3-phosphocholine (DPPC), and 1,2-dimyristoyl-*sn*-glycero-3-phosphocholine (DMPC), with anionic lipids, that is, 1-palmitoyl-2-oleoyl-*sn*-glycero-3-phosphoglycerol (POPG), 1,2-dipalmitoyl-*sn*-glycero-3-phosphoglycerol (DPPG), and 1,2-dimyristoyl-*sn*-glycero-3-phosphoglycerol (DMPG). The lipid composition of the three membranes studied here are 7:3 POPC/POPG, 7:3 DPPC/DPPG, and 7:3 DMPC/DMPG. These bilayers differ in the number of carbon atoms and the number of saturated bonds in their lipid tails, which is 18:0−16:1 for POPC/POPG, 16:0 for DPPC/DPPG, and 14:0 for DMPC/DMPG. This accounts for gel−liquid transition temperatures of ~268, 297.3, and 315.6 K, respectively.[76−78] The CHARMM-GUI suite was used to build these anionic bilayers, wherein sodium ions were added to the solution to account for systems with neutral charge.[79−81] All systems were equilibrated using the two sets of three 5 ps simulations provided by CHARMM-GUI. In the first set, simulations are performed in the *NVT* ensemble with the magnitude of the atomic restrains reduced after each simulation. The second set of simulations is performed in a similar fashion in the *NPT* ensemble.

Simulations starting with peptides deposited on the membrane surface were prepared in a step-by-step approach. In particular, up to three peptides were added to the solution and a short simulation was carried out until they became deposited on the membrane surface.[60] This process was repeated until the desired number of peptides on each membrane surface was attained. During preparation of the simulation and whenever needed, peptides were deleted from the membrane surface, for example, to ensure an equal number of peptides on both membrane leaflets or to ensure that peptides are only deposited on one membrane leaflet. We used the GROMACS suite to insert peptides randomly in the simulations box.[82] Simulations were also performed with a preformed fibrils or tetramers in solution. Table S1 provides a list of all simulations performed in this study.

Some of the simulations were performed on our local cluster using GROMACS-2020[82] with the CHARMM36m force field and the TIP3P water model.[83] The leapfrog algorithm was used to integrate the equations of motion with a time step of 2 fs. Simulations were conducted in the NPT ensemble using a Nóse−Hoover thermostat[84,85] with τ_T = 1 ps and a semi-isotropic Parrinello−Rahman[86] barostat with τ_P = 5 ps. The cutoff for van der Waals interactions was set to be 1.2 nm. Electrostatic interactions were treated using the smooth particle mesh Ewald scheme with a grid spacing of 0.12 and a 1.2 nm real-space cutoff.[87] As shown in Table S1, some of the simulations were executed on an Anton 2 supercomputer.[88]

Analysis. The secondary structure of peptides is determined using the STRIDE algorithm within VMD.[89] In the different trajectories, peptides are found either in a disordered state (most residues are in the coil state) or as a β-strand when interacting with other peptides. Fibrils emerge when non-polar residues of two neighboring β-sheets pack against each other minimizing their exposure to the solvent—see Figure 5. Oligomers are loosely defined in this paper as the structures emerging when three β-sheets in solution pack against each other. Non-polar residues are still largely exposed to the solvent in the latter—see Figure 4.

To estimate the pore diameter, we calculated the average number of water molecules inside a 1 nm height probe inside the pore. Then, assuming the probe to be a cylinder, its diameter was calculated using a radius of 0.14 nm for water molecules. Angles Θ and χ were computed using in-house Python codes using MDTraj package. The deuterium order parameters were computed using the GROMACS suite.

ASSOCIATED CONTENT

Supporting Information

The Supporting Information is available free of charge at https://pubs.acs.org/doi/10.1021/acschemneuro.2c00446.

Animations of membrane damage from two leaflets (MOV)

Animations of membrane damage from a single leaflet (MOV)

Table summarizing the simulations in this study, results of the other simulations with poration from two leaflets, single leaflet, and detergent-like damages, and deuterium order parameters of different types of lipids in the absence of proteins (PDF)

AUTHOR INFORMATION

Corresponding Author

Cristiano L. Dias − *Department of Physics, New Jersey Institute of Technology, Newark, New Jersey 07102-1982, United States;* orcid.org/0000-0002-8765-3922; Email: cld@njit.edu

Authors

Yanxing Yang − *Department of Physics, New Jersey Institute of Technology, Newark, New Jersey 07102-1982, United States;* orcid.org/0000-0003-2521-6441

https://doi.org/10.1021/acschemneuro.2c00446
ACS Chem. Neurosci. 2022, 13, 2766−2777

Hannah Distaffen − *Department of Chemistry, University of Rochester, Rochester, New York 14627, United States*
Sharareh Jalali − *Department of Physics, New Jersey Institute of Technology, Newark, New Jersey 07102-1982, United States*
Andrew J. Nieuwkoop − *Department of Chemistry and Chemical Biology, Rutgers University, Piscataway, New Jersey 08854, United States;* orcid.org/0000-0003-4557-1416
Bradley L. Nilsson − *Department of Chemistry, University of Rochester, Rochester, New York 14627, United States;* orcid.org/0000-0003-1193-3693

Complete contact information is available at: https://pubs.acs.org/10.1021/acschemneuro.2c00446

Author Contributions

Y.Y. and C.L.D. designed the experiments. Y.Y., H.D., A.J.N., and B.L.N. executed the experiments. Y.Y. and S.J. performed the analysis. Y.Y., and C.L.D. wrote the paper.

Notes

The authors declare no competing financial interest.

■ ACKNOWLEDGMENTS

This work was supported by the National Science Foundation under grant nos. CHE-1904364 and CHE-1904528. Computational resources were provided by the Academic and Research Computing System (ARCS) at New Jersey Institute of Technology and by the Pittsburgh Supercomputing Center (PSC). Anton 2 at PSC is supported by the National Instituted of General Medical Sciences of the National Institute of Health under award number R01GM116961. The Anton 2 machine at PSC was generously made available by D. E. Shaw Research.

■ REFERENCES

(1) Owen, M. C.; Gnutt, D.; Gao, M.; Wärmländer, S. K.; Jarvet, J.; Gräslund, A.; Winter, R.; Ebbinghaus, S.; Strodel, B. Effects of in vivo conditions on amyloid aggregation. *Chem. Soc. Rev.* **2019**, *48*, 3946−3996.
(2) Cecchi, C.; Baglioni, S.; Fiorillo, C.; Pensalfini, A.; Liguri, G.; Nosi, D.; Rigacci, S.; Bucciantini, M.; Stefani, M. Insights into the molecular basis of the differing susceptibility of varying cell types to the toxicity of amyloid aggregates. *J. Cell Sci.* **2005**, *118*, 3459−3470.
(3) Julien, C.; Tomberlin, C.; Roberts, C. M.; Akram, A.; Stein, G. H.; Silverman, M. A.; Link, C. D. In vivo induction of membrane damage by β-amyloid peptide oligomers. *Acta Neuropathol. Commun.* **2018**, *6*, 131.
(4) Zasloff, M. Antimicrobial peptides of multicellular organisms. *Nature* **2002**, *415*, 389−395.
(5) Magana, M.; Pushpanathan, M.; Santos, A. L.; Leanse, L.; Fernandez, M.; Ioannidis, A.; Giulianotti, M. A.; Apidianakis, Y.; Bradfute, S.; Ferguson, A. L.; et al. The value of antimicrobial peptides in the age of resistance. *Lancet Infect. Dis.* **2020**, *20*, e216−e230.
(6) Fjell, C. D.; Hiss, J. A.; Hancock, R. E.; Schneider, G. Designing antimicrobial peptides: form follows function. *Nat. Rev. Drug Discovery* **2012**, *11*, 37−51.
(7) López de la Paz, M.; Goldie, K.; Zurdo, J.; Lacroix, E.; Dobson, C. M.; Hoenger, A.; Serrano, L. De novo designed peptide-based amyloid fibrils. *Proc. Natl. Acad. Sci. U.S.A.* **2002**, *99*, 16052−16057.
(8) Tjernberg, L.; Hosia, W.; Bark, N.; Thyberg, J.; Johansson, J. Charge Attraction and β Propensity Are Necessary for Amyloid Fibril Formation from Tetrapeptides. *J. Biol. Chem.* **2002**, *277*, 43243−43246.
(9) Muller, M. P.; Jiang, T.; Sun, C.; Lihan, M.; Pant, S.; Mahinthichaichan, P.; Trifan, A.; Tajkhorshid, E. Characterization of lipid−protein interactions and lipid-mediated modulation of membrane protein function through molecular simulation. *Chem. Rev.* **2019**, *119*, 6086−6161.
(10) Bode, D. C.; Freeley, M.; Nield, J.; Palma, M.; Viles, J. H. Amyloid-β oligomers have a profound detergent-like effect on lipid membrane bilayers, imaged by atomic force and electron microscopy. *J. Biol. Chem.* **2019**, *294*, 7566−7572.
(11) Sasahara, K.; Morigaki, K.; Shinya, K. Effects of membrane interaction and aggregation of amyloid β-peptide on lipid mobility and membrane domain structure. *Phys. Chem. Chem. Phys.* **2013**, *15*, 8929.
(12) Sparr, E.; Engel, M. F.; Sakharov, D. V.; Sprong, M.; Jacobs, J.; de Kruijff, B.; Höppener, J. W.; Antoinette Killian, J. Islet amyloid polypeptide-induced membrane leakage involves uptake of lipids by forming amyloid fibers. *FEBS Lett.* **2004**, *577*, 117−120.
(13) Engel, M. F. M.; Khemtémourian, L.; Kleijer, C. C.; Meeldijk, H. J. D.; Jacobs, J.; Verkleij, A. J.; de Kruijff, B.; Killian, J. A.; Höppener, J. W. M. Membrane damage by human islet amyloid polypeptide through fibril growth at the membrane. *Proc. Natl. Acad. Sci. U.S.A.* **2008**, *105*, 6033−6038.
(14) Reynolds, N. P.; Soragni, A.; Rabe, M.; Verdes, D.; Liverani, E.; Handschin, S.; Riek, R.; Seeger, S. Mechanism of membrane interaction and disruption by α-synuclein. *J. Am. Chem. Soc.* **2011**, *133*, 19366−19375.
(15) Arispe, N.; Rojas, E.; Pollard, H. B. Alzheimer disease amyloid β protein forms calcium channels in bilayer membranes: blockade by tromethamine and aluminum. *Proc. Natl. Acad. Sci. U.S.A.* **1993**, *90*, 567−571.
(16) Arispe, N.; Pollard, H. B.; Rojas, E. β-amyloid Ca^{2+}-channel hypothesis for neuronal death in Alzheimer Disease. *Mol. Cell. Biochem.* **1994**, *140*, 119−125.
(17) Arispe, N.; Pollard, H. B.; Rojas, E. Giant multilevel cation channels formed by Alzheimer disease amyloid beta-protein [A beta P-(1-40)] in bilayer membranes. *Proc. Natl. Acad. Sci. U.S.A.* **1993**, *90*, 10573−10577.
(18) Lipkin, R.; Lazaridis, T. Computational studies of peptide-induced membrane pore formation. *Philos. Trans. R. Soc., B* **2017**, *372*, 20160219.
(19) Gao, M.; Winter, R. The effects of lipid membranes, crowding and osmolytes on the aggregation, and fibrillation propensity of human IAPP. *J. Diabetes Res.* **2015**, *2015*, 1−21.
(20) Pearce, A. K.; O'Reilly, R. K. Polymers for biomedical applications: the importance of hydrophobicity in directing biological interactions and application efficacy. *Biomacromolecules* **2021**, *22*, 4459−4469.
(21) Li, Z.; Pearce, A. K.; Du, J.; Dove, A. P.; O'Reilly, R. K. Uniform antibacterial cylindrical nanoparticles for enhancing the strength of nanocomposite hydrogels. *J. Polym. Sci.* **2022**, 1.
(22) Park, P.; Franco, L. R.; Chaimovich, H.; Coutinho, K.; Cuccovia, I. M.; Lima, F. S. Binding and flip as initial steps for BP-100 antimicrobial actions. *Sci. Rep.* **2019**, *9*, 8622.
(23) Chen, C. H.; Melo, M. C.; Berglund, N.; Khan, A.; de la Fuente-Nunez, C.; Ulmschneider, J. P.; Ulmschneider, M. B. Understanding and modelling the interactions of peptides with membranes: from partitioning to self-assembly. *Curr. Opin. Struct. Biol.* **2020**, *61*, 160−166.
(24) Upadhyay, S. K.; Wang, Y.; Zhao, T.; Ulmschneider, J. P. Insights from micro-second atomistic simulations of melittin in thin lipid bilayers. *J. Membr. Biol.* **2015**, *248*, 497−503.
(25) Wang, Y.; Chen, C. H.; Hu, D.; Ulmschneider, M. B.; Ulmschneider, J. P. Spontaneous formation of structurally diverse membrane channel architectures from a single antimicrobial peptide. *Nat. Commun.* **2016**, *7*, 13535.
(26) Perrin, B. S., Jr.; Fu, R.; Cotten, M. L.; Pastor, R. W. Simulations of membrane-disrupting peptides II: AMP piscidin 1 favors surface defects over pores. *Biophys. J.* **2016**, *111*, 1258−1266.
(27) Fatafta, H.; Khaled, M.; Owen, M. C.; Sayyed-Ahmad, A.; Strodel, B. Amyloid-β peptide dimers undergo a random coil to β-sheet transition in the aqueous phase but not at the neuronal membrane. *Proc. Natl. Acad. Sci. U.S.A.* **2021**, *118*, 118.

(28) Banerjee, S.; Hashemi, M.; Zagorski, K.; Lyubchenko, Y. L. Cholesterol in membranes facilitates aggregation of amyloid β protein at physiologically relevant concentrations. *ACS Chem. Neurosci.* **2021**, *12*, 506−516.
(29) Brown, A. M.; Bevan, D. R. Molecular dynamics simulations of amyloid β-peptide (1-42): Tetramer formation and membrane interactions. *Biophys. J.* **2016**, *111*, 937−949.
(30) Ermilova, I.; Lyubartsev, A. P. Modelling of interactions between Aβ (25−35) peptide and phospholipid bilayers: effects of cholesterol and lipid saturation. *RSC Adv.* **2020**, *10*, 3902−3915.
(31) Lipkin, R.; Pino-Angeles, A.; Lazaridis, T. Transmembrane pore structures of β-hairpin antimicrobial peptides by all-atom simulations. *J. Phys. Chem. B* **2017**, *121*, 9126−9140.
(32) Connelly, L.; Jang, H.; Teran Arce, F.; Capone, R.; Kotler, S. A.; Ramachandran, S.; Kagan, B. L.; Nussinov, R.; Lal, R. Atomic force microscopy and MD simulations reveal pore-like structures of all-d-Enantiomer of Alzheimer's β-amyloid peptide: relevance to the ion channel mechanism of AD pathology. *J. Phys. Chem. B* **2012**, *116*, 1728−1735.
(33) Connelly, L.; Jang, H.; Teran Arce, F.; Ramachandran, S.; Kagan, B. L.; Nussinov, R.; Lal, R. Effects of point substitutions on the structure of toxic Alzheimer's β-amyloid channels: atomic force microscopy and molecular dynamics simulations. *Biochemistry* **2012**, *51*, 3031−3038.
(34) Quist, A.; Doudevski, I.; Lin, H.; Azimova, R.; Ng, D.; Frangione, B.; Kagan, B.; Ghiso, J.; Lal, R. Amyloid ion channels: a common structural link for protein-misfolding disease. *Proc. Natl. Acad. Sci. U.S.A.* **2005**, *102*, 10427−10432.
(35) Dong, X.; Qiao, Q.; Qian, Z.; Wei, G. Recent computational studies of membrane interaction and disruption of human islet amyloid polypeptide: Monomers, oligomers and protofibrils. *Biochim. Biophys. Acta, Biomembr.* **2018**, *1860*, 1826−1839.
(36) Sun, D.; Forsman, J.; Woodward, C. E. Molecular simulations of melittin-induced membrane pores. *J. Phys. Chem. B* **2017**, *121*, 10209−10214.
(37) Pino-Angeles, A.; Lazaridis, T. Effects of peptide charge, orientation, and concentration on melittin transmembrane pores. *Biophys. J.* **2018**, *114*, 2865−2874.
(38) Ngo, S. T.; Hung, H. M.; Tran, K. N.; Nguyen, M. T. Replica exchange molecular dynamics study of the amyloid beta (11-40) trimer penetrating a membrane. *RSC Adv.* **2017**, *7*, 7346−7357.
(39) Liu, Y.; Ren, B.; Zhang, Y.; Sun, Y.; Chang, Y.; Liang, G.; Xu, L.; Zheng, J. Molecular simulation aspects of amyloid peptides at membrane interface. *Biochim. Biophys. Acta, Biomembr.* **2018**, *1860*, 1906−1916.
(40) Leveritt, J. M., III; Pino-Angeles, A.; Lazaridis, T. The structure of a melittin-stabilized pore. *Biophys. J.* **2015**, *108*, 2424−2426.
(41) Mihajlovic, M.; Lazaridis, T. Antimicrobial peptides in toroidal and cylindrical pores. *Biochim. Biophys. Acta, Biomembr.* **2010**, *1798*, 1485−1493.
(42) Pino-Angeles, A.; Leveritt, J. M., III; Lazaridis, T. Pore structure and synergy in antimicrobial peptides of the magainin family. *PLoS Comput. Biol.* **2016**, *12*, No. e1004570.
(43) Mihailescu, M.; Sorci, M.; Seckute, J.; Silin, V. I.; Hammer, J.; Perrin, B. S., Jr; Hernandez, J. I.; Smajic, N.; Shrestha, A.; Bogardus, K. A.; et al. Structure and function in antimicrobial piscidins: histidine position, directionality of membrane insertion, and pH-dependent permeabilization. *J. Am. Chem. Soc.* **2019**, *141*, 9837−9853.
(44) Herce, H. D.; Garcia, A. E. Molecular dynamics simulations suggest a mechanism for translocation of the HIV-1 TAT peptide across lipid membranes. *Proc. Natl. Acad. Sci. U.S.A.* **2007**, *104*, 20805−20810.
(45) Leontiadou, H.; Mark, A. E.; Marrink, S. J. Antimicrobial peptides in action. *J. Am. Chem. Soc.* **2006**, *128*, 12156−12161.
(46) Jang, H.; Zheng, J.; Nussinov, R. Models of beta-amyloid ion channels in the membrane suggest that channel formation in the bilayer is a dynamic process. *Biophys. J.* **2007**, *93*, 1938−1949.
(47) Jang, H.; Arce, F. T.; Ramachandran, S.; Capone, R.; Azimova, R.; Kagan, B. L.; Nussinov, R.; Lal, R. Truncated β-amyloid peptide channels provide an alternative mechanism for Alzheimer's Disease and Down syndrome. *Proc. Natl. Acad. Sci. U.S.A.* **2010**, *107*, 6538−6543.
(48) Jang, H.; Connelly, L.; Teran Arce, F.; Ramachandran, S.; Kagan, B. L.; Lal, R.; Nussinov, R. Mechanisms for the Insertion of Toxic, Fibril-like β-Amyloid Oligomers into the Membrane. *J. Chem. Theory Comput.* **2012**, *9*, 822−833.
(49) Chang, Z.; Luo, Y.; Zhang, Y.; Wei, G. Interactions of Aβ25- 35 β-Barrel-like oligomers with anionic lipid bilayer and resulting membrane leakage: an all-atom molecular dynamics study. *J. Phys. Chem. B* **2011**, *115*, 1165−1174.
(50) Gupta, K.; Jang, H.; Harlen, K.; Puri, A.; Nussinov, R.; Schneider, J. P.; Blumenthal, R. Mechanism of Membrane Permeation Induced by Synthetic β-Hairpin Peptides. *Biophys. J.* **2013**, *105*, 2093−2103.
(51) Sciacca, M. F.; Kotler, S. A.; Brender, J. R.; Chen, J.; Lee, D.-k.; Ramamoorthy, A. Two-step mechanism of membrane disruption by A-β through membrane fragmentation and pore formation. *Biophys. J.* **2012**, *103*, 702−710.
(52) Sciacca, M. F.; Milardi, D.; Messina, G. M.; Marletta, G.; Brender, J. R.; Ramamoorthy, A.; La Rosa, C. L. Cations as switches of amyloid-mediated membrane disruption mechanisms: calcium and IAPP. *Biophys. J.* **2013**, *104*, 173−184.
(53) Sciacca, M. F. M.; Monaco, I.; La Rosa, C.; Milardi, D. The active role of Ca^{2+} ions in Aβ-mediated membrane damage. *Chem. Commun.* **2018**, *54*, 3629−3631.
(54) Sciacca, M. F.; Lolicato, F.; Tempra, C.; Scollo, F.; Sahoo, B. R.; Watson, M. D.; García-Viñuales, S.; Milardi, D.; Raudino, A.; Lee, J. C.; Ramamoorthy, A.; La Rosa, C. Lipid-chaperone hypothesis: a common molecular mechanism of membrane disruption by intrinsically disordered proteins. *ACS Chem. Neurosci.* **2020**, *11*, 4336−4350.
(55) Vargas, J.; Alarcón, J.; Rojas, E. Displacement currents associated with the insertion of Alzheimer disease amyloid β-Peptide into planar bilayer membranes. *Biophys. J.* **2000**, *79*, 934−944.
(56) Lau, T. L.; Ambroggio, E. E.; Tew, D. J.; Cappai, R.; Masters, C. L.; Fidelio, G. D.; Barnham, K. J.; Separovic, F. Amyloid-beta peptide disruption of lipid membranes and the effect of metal ions. *J. Mol. Biol.* **2006**, *356*, 759−770.
(57) Bowerman, C. J.; Nilsson, B. L. A reductive trigger for peptide self-assembly and hydrogelation. *J. Am. Chem. Soc.* **2010**, *132*, 9526−9527.
(58) Jalali, S.; Yang, Y.; Mahmoudinobar, F.; Singh, S. M.; Nilsson, B. L.; Dias, C. Using all-atom simulations in explicit solvent to study aggregation of amphipathic peptides into amyloid-like fibrils. *J. Mol. Liq.* **2022**, *347*, 118283.
(59) Marini, D. M.; Hwang, W.; Lauffenburger, D. A.; Zhang, S.; Kamm, R. D. Left-handed helical ribbon intermediates in the self-assembly of a β-sheet peptide. *Nano Lett.* **2002**, *2*, 295−299.
(60) Yang, Y.; Jalali, S.; Nilsson, B. L.; Dias, C. L. Binding mechanisms of amyloid-like peptides to lipid bilayers and effects of divalent cations. *ACS Chem. Neurosci.* **2021**, *12*, 2027−2035.
(61) Narayanan, C.; Dias, C. L. Hydrophobic interactions and hydrogen bonds in β-sheet formation. *J. Chem. Phys.* **2013**, *139*, 09B640_1. DOI: 10.1063/1.4821596
(62) Su, Z.; Dias, C. L. Driving β-strands into fibrils. *J. Phys. Chem. B* **2014**, *118*, 10830−10836.
(63) Seelig, J. Deuterium magnetic resonance: theory and application to lipid membranes. *Q. Rev. Biophys.* **1977**, *10*, 353−418.
(64) Chau, P.-L.; Hardwick, A. J. A new order parameter for tetrahedral configurations. *Mol. Phys.* **1998**, *93*, 511−518.
(65) Hung, A.; Yarovsky, I. Inhibition of peptide aggregation by lipids: insights from coarse-grained molecular simulations. *J. Mol. Graph. Model.* **2011**, *29*, 597−607.
(66) Brummel, B. E.; Braun, A. R.; Sachs, J. N. Polyunsaturated chains in asymmetric lipids disorder raft mixtures and preferentially associate with α-synuclein. *Biochim. Biophys. Acta, Biomembr.* **2017**, *1859*, 529−536.
(67) LaFerla, F. M.; Green, K. N.; Oddo, S. Intracellular amyloid-β in Alzheimer's disease. *Nat. Rev. Neurosci.* **2007**, *8*, 499−509.

(68) Gyure, K. A.; Durham, R.; Stewart, W. F.; Smialek, J. E.; Troncoso, J. C. Intraneuronal Aβ-Amyloid Precedes Development of Amyloid Plaques in Down Syndrome. *Arch. Pathol. Lab Med.* **2001**, *125*, 489−492.
(69) Gouras, G. K.; Tsai, J.; Naslund, J.; Vincent, B.; Edgar, M.; Checler, F.; Greenfield, J. P.; Haroutunian, V.; Buxbaum, J. D.; Xu, H.; Greengard, P.; Relkin, N. R. Intraneuronal Aβ42 accumulation in human brain. *Am. J. Pathol.* **2000**, *156*, 15−20.
(70) Grudzielanek, S.; Smirnovas, V.; Winter, R. The effects of various membrane physical−chemical properties on the aggregation kinetics of insulin. *Chem. Phys. Lipids* **2007**, *149*, 28−39.
(71) Dias, C. L.; Jalali, S.; Yang, Y.; Cruz, L. Role of Cholesterol on Binding of Amyloid Fibrils to Lipid Bilayers. *J. Phys. Chem. B* **2020**, *124*, 3036−3042.
(72) Zhang, X.; Clair, St. J. R.; London, E.; Raleigh, D. P. Islet amyloid polypeptide membrane interactions: effects of membrane composition. *Biochemistry* **2017**, *56*, 376−390.
(73) Drolle, E.; Negoda, A.; Hammond, K.; Pavlov, E.; Leonenko, Z. Changes in lipid membranes may trigger amyloid toxicity in Alzheimer's disease. *PLoS One* **2017**, *12*, No. e0182194.
(74) Stefani, M.; Liguri, G. Cholesterol in Alzheimer's disease: unresolved questions. *Curr. Alzheimer Res.* **2009**, *6*, 15−29.
(75) Wang, F.; Gnewou, O.; Wang, S.; Osinski, T.; Zuo, X.; Egelman, E. H.; Conticello, V. P. Deterministic chaos in the self-assembly of sheet nanotubes from an amphipathic oligopeptide. *Matter* **2021**, *4*, 3217−3231.
(76) Lewis, R. N.; Zhang, Y.-P.; McElhaney, R. N. Calorimetric and spectroscopic studies of the phase behavior and organization of lipid bilayer model membranes composed of binary mixtures of dimyristoylphosphatidylcholine and dimyristoylphosphatidylglycerol. *Biochim. Biophys. Acta, Biomembr.* **2005**, *1668*, 203−214.
(77) Oliva, R.; Chino, M.; Pane, K.; Pistorio, V.; De Santis, A. D.; Pizzo, E.; D'Errico, G.; Pavone, V.; Lombardi, A.; Del Vecchio, P. D.; Notomista, E.; Nastri, F.; Petraccone, L. Exploring the role of unnatural amino acids in antimicrobial peptides. *Sci. Rep.* **2018**, *8*, 8888.
(78) Macdonald, P. M.; Seelig, J. Calcium binding to mixed phosphatidylglycerol-phosphatidylcholine bilayers as studied by deuterium nuclear magnetic resonance. *Biochemistry* **1987**, *26*, 1231−1240.
(79) Lee, J.; Cheng, X.; Swails, J. M.; Yeom, M. S.; Eastman, P. K.; Lemkul, J. A.; Wei, S.; Buckner, J.; Jeong, J. C.; Qi, Y.; et al. CHARMM-GUI input generator for NAMD, GROMACS, AMBER, OpenMM, and CHARMM/OpenMM simulations using the CHARMM36 additive force field. *J. Chem. Theory Comput.* **2016**, *12*, 405−413.
(80) Jo, S.; Kim, T.; Iyer, V. G.; Im, W. CHARMM-GUI: a web-based graphical user interface for CHARMM. *J. Comput. Chem.* **2008**, *29*, 1859−1865.
(81) Jo, S.; Lim, J. B.; Klauda, J. B.; Im, W. CHARMM-GUI membrane builder for mixed bilayers and its application to yeast membranes. *Biophys. J.* **2009**, *97*, 50−58.
(82) Abraham, M. J.; Murtola, T.; Schulz, R.; Páll, S.; Smith, J. C.; Hess, B.; Lindahl, E. GROMACS: High performance molecular simulations through multi-level parallelism from laptops to supercomputers. *SoftwareX* **2015**, *1−2*, 19−25.
(83) Klauda, J. B.; Venable, R. M.; Freites, J. A.; O'Connor, J. W.; Tobias, D. J.; Mondragon-Ramirez, C.; Vorobyov, I.; MacKerell, A. D.; Pastor, R. W. Update of the CHARMM all-atom additive force field for lipids: validation on six lipid types. *J. Phys. Chem. B* **2010**, *114*, 7830−7843.
(84) Nosé, S. A unified formulation of the constant temperature molecular dynamics methods. *J. Chem. Phys.* **1984**, *81*, 511−519.
(85) Hoover, W. G. Canonical dynamics: Equilibrium phase-space distributions. *Phys. Rev. A* **1985**, *31*, 1695−1697.
(86) Parrinello, M.; Rahman, A. Polymorphic transitions in single crystals: a new molecular dynamics method. *J. Appl. Phys.* **1981**, *52*, 7182−7190.
(87) Darden, T.; York, D.; Pedersen, L. Particle mesh Ewald: an Nlog(N) method for Ewald sums in large systems. *J. Chem. Phys.* **1993**, *98*, 10089−10092.
(88) Shaw, D. E.; Grossman, J.; et al. Anton 2: raising the bar for performance and programmability in a special-purpose molecular dynamics supercomputer *SC'14: Proceedings of the International Conference for High Performance Computing, Networking, Storage and Analysis*, 2014; pp 41−53.
(89) Frishman, D.; Argos, P. Knowledge-based protein secondary structure assignment. *Proteins* **1995**, *23*, 566−579.

https://doi.org/10.1021/acschemneuro.2c00446
ACS Chem. Neurosci. 2022, 13, 2766−2777